Multi-Dimensional Polarized Modulation for Land Mobile Satellite Communications

Liangxin Qian, Ping Yang, *Senior Member, IEEE*, Yong Liang Guan, *Senior Member, IEEE*, Zilong Liu, *Senior Member, IEEE*, Yue Xiao, *Member, IEEE*, Ke Jiang, and Ming Xiao, *Senior Member, IEEE*

***Abstract*—In this paper, a novel multiple-input multiple-out (MIMO) transmission scheme, called generalized polarized enhanced spatial modulation (GPESM), is proposed for dual-polarized land mobile satellite (LMS) communications. We first introduce the enhanced spatial modulation (ESM) technique for dual-polarized LMS communications, in which polarization dimension, spatial dimension and multiple signal constellations are used to transmit information and obtain substantial performance gain. Meanwhile, the theoretical upper bound for the average bit error probability (ABEP) of the proposed GPESM scheme is derived. In order to further improve the reliability of the system, we also propose two novel power allocation (PA) algorithms for GPESM system, which are the optimization-driven approximated max-min distance (AMMD)-based PA algorithm and the data-driven deep neural network (DNN)-based PA algorithm. To achieve an enhanced spatial diversity gain, we consider to apply a reconfigurable intelligent surface (RIS) to the GPESM system as a relay to assist in transmitting information. In this way, the user can receive the information transmitted by the satellite on one hand, and the information sent by the satellite via the RIS relay on the other hand. We also extend the above-mentioned two PA algorithms to the RIS-assisted GPESM systems. Our simulation results show that the RIS-assisted GPESM systems are capable of obtaining high bit error rate (BER) performance gain (up to 10 dB) compared to the standard GPESM system and two PA algorithms can further improve the performance to the systems.**

***Index Terms*—Deep neural network, land mobile satellite, polarized modulation, power allocation, reconfigurable intelligent surfaces.**

I. Introduction

As the fifth generation mobile networks (5G) becomes commercially available, the research community has started to investigate the 6G. The latter will be not only limited to the ground, but also extended to the space and the sea to achieve ubiquitous and seamless connections between the ground, satellite and airborne networks [1]–[3]. Driven by this trend, in recent years, satellite communications have gained renewed interest with reduced satellite deployment costs and breakthroughs in materials and antenna technology [2]. Space-earth integration network has become a key issue in future 6G wireless networks. While the existing terrestrial cellular network technologies may be vulnerable to disasters and terrorist attacks, satellite platforms have a wide range of coverage and broadcast capabilities and can compensate the weakness of terrestrial platforms [2]–[4]. More notably, with commercial satellite companies investing heavily in the satellite industry, satellite platforms have become an important part of the internet-to-things (IoT) [1], [5]. In [3], unmanned aerial vehicle (UAV)-based low-altitude platforms (LAP) can be quickly deployed and flexibly adjusted to the optimal communication environment to achieve better bit error rate (BER) performance and energy efficiency in short-range communications. To address the large amount of data satellites in future, edge intelligent computing has been proposed in [5] for satellite IoT.

Future satellite platforms are promising, yet the capabilities of individual satellites are very limited. On the other hand, MIMO has become a mature technology in terrestrial communication networks, which provides high channel capacity and significant performance improvements [6]. By bringing the MIMO idea to satellite communication platforms, [7] and [8] investigated how to construct a capacity-optimized MIMO channel between two geostationary satellites and ground antennas, which is geometrically and optimally arranged to obtain multiplexed gain from the antennas. [9] and [10] examined the possible capacity of a dual-satellite diagonal MIMO system for frequencies above 10 GHz under correlated rainfall fading. A technique aimed at mitigating interference by using linear precoding of the transmitted signal was proposed in [11]. However, in the satellite communication scenario, the line-of-sight (LOS) propagation, the lack of multipath factors and the absence of scatters may lead to highly correlated spatial components, which further results in an inherent rank deficiency of the MIMO channel matrix.

To address these difficulties, polarization modulation (PMod) was proposed to exploit the dimension of polarization in [12], [13]. For example, the authors of [13] investigated the application of PMod to improve the throughput of mobile satellite communication transmissions, and proved that PMod can achieve 100% through-

L. Qian, P. Yang, Y. Xiao and K. Jiang are with the National Key Laboratory of Science and Technology on Communications, University of Electronic Science and Technology of China 611731, Sichuan, China. L. Qian and P. Yang are also with the State Key Laboratory of Integrated Services Networks, Xidian University. (e-mail: 201921220237@std.uestc.edu.cn; yang.ping@uestc.edu.cn; xiaoyue@uestc.edu.cn; jiangke@std.uestc.edu.cn).

Y. L. Guan is with the School of Electrical and Electronic Engineering, Nanyang Technological University, Singapore. (e-mail: eylguan@ntu.edu.sg).

Z. Liu is with the School of Computer Science and Electronics Engineering, University of Essex, UK. (e-mail: zilong.liu@essex.ac.uk).

M. Xiao is with the information science and engineering (ISE) department, School of Electrical Engineering, KTH, Sweden. (e-mail: mingx@kth.se).

This work is supported by the National Science Foundation of China under Grant number 61876033, the Open Project of State Key Laboratory of Integrated Services Networks of Xidian University under Grant number ISN21-14, and the National Science Foundation of China under Grant number U19B2014.

put improvement relative to existing deployments. In [14], based on accurate experimental results, the statistical modeling of dual-polarized satellite MIMO fading channels was addressed, which is useful for the design and performance assessment of MIMO-land mobile satellite (LMS) transmission systems. The model given in [14] was further developed in [15] by considering more critical channel aspects. Recently, [16] introduced orthogonal space-time block coding (OSTBC) into PMod MIMO-LMS communications to achieve a high spatial diversity. In [17], a novel multi-dimensional PMod scheme was proposed by employing the 3-D constellations, rather than the classic approach of 2-D. In [18], the PMod scheme was combined with the directional polarization modulation method to enhance the transmission security in MIMO-LMS communications.

Most recently, the concept of index modulation (IM), i.e., spatial modulation (SM)-MIMO, has been applied to dual-polarized satellite MIMO systems [19], [20]. Specifically, in [19], the polarization domain was used to represent information and only a single polarized antenna was activated in each time slot. It is shown in [19] that the proposed polarized modulation (PM) is capable of avoiding cross polarization interference (CPI) and mitigating the possibility of inter-beam interference. [20] further presented two SM schemes for dual-polarized MIMO-LMS systems, namely generalized polarized modulation (GPMod) and polarized spatial modulation (PMod-SM), aiming at circumventing the CPI while maintaining a high transmit rate. Moreover, in [21], a novel multi-domain modulation architecture was proposed, where the polarization dimension was added to conventional SM mappings, by considering the generalized spatially correlated Rayleigh and Rician fading channel models. A novel PMod scheme, namely dual-polarized spatial media-based modulation was proposed in [22], which combines the benefits of the media-based modulation (MBM), spatial modulation (SM), and dual-polarized (DP) antennas. Among the promising PMod design alternatives for MIMO-LMS communications, the enhanced spatial modulation (ESM) techniques constitute an attractive multi-dimensional PMod regime [23], which extends the conventional SM by introducing a series of signal constellations and uses antenna indices and multiple signal constellations to transfer information. In ESM, the properly designed primary and secondary constellations bring an improvement of BER performance compared to conventional SM-based designs. To the best of our knowledge, none of the existing studies on ESM for MIMO-LMS communications have been reported.

Power allocation (PA) is a common method of enhancing system performance in MIMO systems, while providing the flexibility to allocate power resources based on the available channel information. Recently, various PA algorithms were proposed for the SM-based communication systems. For example, [24] proposed two PA algorithms for receive spatial modulation (RSM) MIMO systems, which are designed based on the error vector reduction (EVR) method and iterative optimization algorithm, respectively. In [25], the PA algorithm was combined with the transmit antenna selection algorithm for SM, where the deep neural networks (DNN) was employed as the problem solver. Compared to these link adaption algorithms, recent studies have shown that reconfigurable intelligent surfaces (RIS) can accurately control the communication propagation environment to greatly enhance signal quality at the receiver [26]–[28]. RIS is an artificial electromagnetic surface that can change the phases, amplitudes, and polarizations of propagation signals. This technology advocates the concept of "smart radio environments", which is distinctively different from the current uncontrolled communication environment. RIS is widely conceived as a potential technology for enhanced communication systems in 6G.

Against the above background, we summarize the main contributions of this paper as follows:

1) We introduce the ESM technology into the dual-polarized dual-satellite MIMO-LMS communication systems, and propose a novel PMod scheme, namely generalized polarized enhanced spatial modulation (GPESM). To reduce the CPI, the two transmitting antennas of the two satellites choose as different polarization methods as possible. This means that only one antenna with one polarization per time slot is selected to transmit the signal or two antennas with different polarizations are selected to transmit the signal. Meanwhile, the theoretical upper bound for average bit error probability (ABEP) of the proposed GPESM scheme is derived. Simulation results have verified the advantages of GPESM.
2) In order to further improve the reliability of the GPESM scheme, we propose two PA methods for GPESM, which are based on optimization-driven approximated maximum minimum distance (AMMD) and data-driven DNN, respectively. We provide BER performance and complexity comparison for these two PA methods.
3) To maximize the use of the freedom provided by RIS, we introduce a novel GPESM transmission scheme for dual-polarized MIMO-LMS communications. In our proposed scheme, the RIS takes discrete amplitude and phase values from a fixed set of reflection parameters, which does not need to know the transmitter information. Moreover, we also apply the proposed two PA algorithms to the RIS-assisted GPESM systems. Numerical results show that the proposed RIS-assisted GPESM systems are capable of achieving considerable performance gains (up to 10 dB) compared to conventional GPESM systems.

The organization of this paper is as follows: The statistical dual-polarized LMS MIMO channel model is presented in Section II. In Section III, the concepts of GPMod and GPESM are introduced, and the maximum-likelihood (ML) detection and BER performance analysis are also provided. Two PA strategies for GPESM and RIS-assisted GPESM schemes are provided in Section IV. The simulation results and BER performances are presented in Section V. Section VI concludes this paper.

Notation: Boldface capital and lowercase symbols represent matrices and column vectors, respectively. The $(\cdot)^T$ and $(\cdot)^H$ operations represent transpose and Hermitian transpose, respectively. The real number field is represented by $\mathbb{R}$. The complex number field is represented by

$\mathbb{C}$. real$(\cdot)$ is the real-part operator. $\|\cdot\|$ stands for the Frobenius norm. diag$\{\cdot\}$ refers to the diagonal operation. $Tr(\cdot)$ returns the trace of a square matrix. $E(\cdot)$ represents the expectation operator. $vec(\cdot)$ refers to the vectorization of a matrix, which is a linear transformation of converting the matrix into a column vector. $Q(\cdot)$ is the Q-function. $P_b(\cdot)$ denotes the average bit error probability operator. $P(\cdot)$ denotes the probability operator. $\odot$ represents the Hadamard product. $d(\cdot)$ is Hamming distance. $D(\cdot)$ is minimum squared Euclidian distance.

II. Statistical Dual-Polarized LMS MIMO Channel Model

In this paper, MIMO LMS channel scenarios are considered, where a single satellite uses a dual circularly polarized antenna with a right- and left-hand circular polarized (R/LHCP) element and the mobile user terminal (UT) is also fitted with a similar dual circularly polarized antenna. We stipulate $N_t = 1$ and $N_r = 1$ in the transceiver system of a single dual circular polarized antenna. Since each dual circularly polarized antenna has two polarization modes, the transceiver system of a single dual circularly polarized antenna can be regarded as a 2×2 MIMO system. For each dual-polarized MIMO LMS channel (each transmitter to receiver link), it can be modeled by a 2×2 MIMO channel matrix $\mathbf{H} = [h_{ij}]$ $(i,\, j = 1,\, 2)$, where h_{ij} $(i,j = 1,2)$ represent the fading components of the SISO LMS subchannel formed between the transmit and receive sides, which incorporate both the large-scale fading effects and the small-scale fading effects. Under these assumptions, each LMS MIMO channel can be expressed as

$$\begin{aligned}\mathbf{H} = [h_{ij}] &= \sqrt{\tfrac{K}{1+K}}[\bar{h}_{ij}] + \sqrt{\tfrac{1}{1+K}}[\tilde{h}_{ij}] \\ &= \sqrt{\tfrac{K}{1+K}}\bar{\mathbf{H}} + \sqrt{\tfrac{1}{1+K}}\tilde{\mathbf{H}},\end{aligned} \tag{1}$$

where K is the Rician factor, $\bar{\mathbf{H}}$ and $\tilde{\mathbf{H}}$ are the static line-of-sight (LOS) component and the variable non-LOS component, respectively. In (1), the elements of the channel matrix $\mathbf{H}$ can be expressed as

$$\begin{aligned}h_{ij} &= |h_{i,j}|\exp(j\phi_{ij}) \\ &= \sqrt{\tfrac{K}{1+K}}|\bar{h}_{i,j}|\exp(j\bar{\phi}_{ij}) + \sqrt{\tfrac{1}{1+K}}|\tilde{h}_{i,j}|\exp(j\tilde{\phi}_{ij}),\end{aligned} \tag{2}$$

where the phases $\bar{\phi}_{ij}$ and $\tilde{\phi}_{ij}$ are uniformly distributed over the range of $[0,\, 2\pi]$, while the magnitudes $|\bar{h}_{i,j}|$ are log-normally distributed determined by specific distribution parameters $(\alpha,\, \psi)$ (α is the mean and ψ is the standard deviation) and the magnitudes $|\tilde{h}_{i,j}|$ are Rayleigh distributed with the multipath power parameter ω. Different environments, polarizations and elevation angles θ are capable of affecting the values of $(\alpha,\ \psi, \omega)$. In general, for some classic models, these parameters can be selected based on the experimental results given in [15].

In 2×2 dual-polarized LMS MIMO systems, as shown in Fig. 1 (a), the spatial correlation of the large scale fading component $\bar{\mathbf{H}}$ is given by

$$vec(\bar{\mathbf{H}}) = 10^{[vec(\bar{\mathbf{H}}_w)\cdot(\psi/20)\cdot\bar{\mathbf{C}}^{1\,/\,2}+(\alpha/20)]}, \tag{3}$$

where $\bar{\mathbf{H}}_w$ is the 2×2 channel matrix with spatial uncorrelated, identically distributed, circularly symmetric complex Gaussian elements of zero mean and unit variance and $\bar{\mathbf{C}}$ is the 4×4 positive semi-definite Hermitian covariance matrix of large scale fading components.

On the other hand, the spatial correlation of small scale fading component $\tilde{\mathbf{H}}$ is generated as [34]

$$\tilde{\mathbf{H}} = \tilde{R}_{\mathrm{rx}}^{1/2}\cdot\tilde{\mathbf{H}}_w\cdot R_{\mathrm{tx}}^{1/2}, \tag{4}$$

where $\tilde{\mathbf{H}}_w$ is the 2×2 channel matrix with spatial uncorrelated, identically distributed, circularly symmetric complex Gaussian elements of zero mean and ω variance. $\tilde{R}_{\mathrm{rx}}$ and $\tilde{R}_{\mathrm{tx}}$ denote the receive covariance matrix and transmit covariance matrix, respectively. $\tilde{R}_{\mathrm{rx}}$ and $\tilde{R}_{\mathrm{tx}}$ can be expressed as

$$\begin{aligned}\tilde{R}_{\mathrm{rx}} &= E[\tilde{\mathbf{H}}^H\tilde{\mathbf{H}}] \\ &= \omega\cdot\begin{bmatrix} 1 & 2\tilde{\rho}_{\mathrm{rx}}\sqrt{(1-\gamma)\gamma} \\ 2\tilde{\rho}_{\mathrm{rx}}\sqrt{(1-\gamma)\gamma} & 1\end{bmatrix},\end{aligned} \tag{5}$$

$$\begin{aligned}\tilde{R}_{\mathrm{tx}} &= E[\tilde{\mathbf{H}}^H\tilde{\mathbf{H}}] \\ &= \omega\cdot\begin{bmatrix} 1 & 2\tilde{\rho}_{\mathrm{tx}}\sqrt{(1-\gamma)\gamma} \\ 2\tilde{\rho}_{\mathrm{tx}}\sqrt{(1-\gamma)\gamma} & 1\end{bmatrix},\end{aligned} \tag{6}$$

where $\tilde{\rho}_{\mathrm{rx}}$ and $\tilde{\rho}_{\mathrm{tx}}$ are the small-scale polarization correlation coefficients at the receiver and transmitter, respectively. The value of γ can be formulated as

$$\gamma = \beta_{\mathrm{ant}}(1-\beta_{\mathrm{env}}) + (1-\beta_{\mathrm{ant}})\beta_{\mathrm{env}}, \tag{7}$$

where $\omega_{\mathrm{ant}} = 10\log_{10}[(1-\beta_{\mathrm{ant}})/\beta_{\mathrm{ant}}]$ is the cross-polar discrimination of transmit antennas (TA) and $\omega_{\mathrm{env}} = 10\log_{10}[(1-\beta_{\mathrm{env}})/\beta_{\mathrm{env}}]$ is the cross-polar coupling in the transmission environment. In general, the ranges of the parameters β_{ant} and β_{env} are $[0, 1]$ and their suitable values depend on ω_{ant} and ω_{env}.

Note that based on the model given in (1)-(7), when multiple satellites (such the system shown in Fig. 1 (b)) are considered, the LMS channel matrix $\mathbf{H}$, can be further defined as

$$\mathbf{H} = [\mathbf{H}_1\cdots\mathbf{H}_N], \tag{8}$$

where $\mathbf{H}_k$, $k = 1,\cdots,N$ is the independent 2×2 channel matrix from the kth satellite to the user terminal.

III. System Model

A. GPMod Preview

In the GPMod structure, $M_1 + M_2$ bits are sent over one GPMod symbol, where the first M_1 bits are utilized to select a specific PSK/QAM constellation point, while the remaining M_2 bits are used to select the specific polarizations of the transmit antennas (For dual-polarized LMS systems, each transmit antenna has two states). For example, for the dual-polarized two-antenna ($N_t = 2$ and $N_r = 1$) LMS-MIMO system with BPSK modulation, the number of bits conveyed by each GPMod symbol is $\log_2(2N_t) + \log_2(2) = 3$. All possible three-bit combinations $\{000, 001, 010, 011, 100, 101, 110, 111\}$ are mapped to the indices of transmit antenna polarization (i.e., LHCP or RHCP) and to the BPSK constellation $\{+1, -1\}$, e.g. the LHCP state of the first TA is activated to transmit the BPSK constellation point "-1", when the input bits are $\{000\}$.

According to the above concept, the general system model of GPMod can be formulated by

$$\mathbf{y} = \mathbf{H}\mathbf{c}s + \mathbf{n}, \tag{9}$$

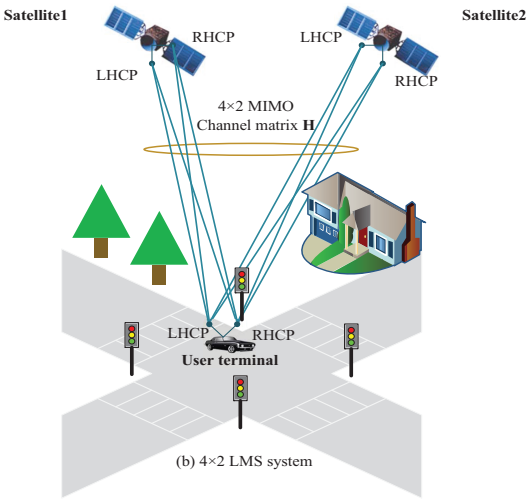

Fig. 1. Dual-polarized LMS MIMO system.

TABLE I
GPMod mapping rule for 3 bits/s/Hz transmission using BPSK for dual polarized dual satellite systems, where "X" denotes one bit conveyed by PSK symbols.

Transmit bits	Satellite1-LHCP	Satellite1-RHCP	Satellite2-LHCP	Satellite2-RHCP
X00	BPSK	0	BPSK	0
X01	BPSK	0	0	BPSK
X10	0	BPSK	BPSK	0
X11	0	BPSK	0	BPSK

where $\mathbf{y} \in \mathbb{C}^{2N_r \times 1}$ is the received signal, $\mathbf{H} \in \mathbb{C}^{2N_r \times 2N_t}$ is the dual-polarized MIMO-LMS channel matrix, and $\mathbf{c} \in \mathbb{R}^{2N_t \times 1}$ is the transmit signal matrix (namely state active matrix) corresponding to the selection of the transmit antenna polarization, which can be given by

$$\mathbf{c} = \begin{bmatrix} 1-c_1 \\ c_1 \\ 1-c_2 \\ c_2 \end{bmatrix}, \tag{10}$$

where the legitimate values of c_1 and c_2 are in the binary set of $\{0, 1\}$. In (9), s is the transmitted PSK/QAM constellation point and $\mathbf{n} \in \mathbb{C}^{2N_r \times 1}$ is the zero mean vector of additive complex Gaussian noise (AWGN) with i.i.d. elements and variance of σ^2. Thus, when the total number of transmit antennas is two, i.e., for the case of one satellite having two TAs or two satellites equipped with a single TA, the system model can also be re-formulated to

$$\begin{bmatrix} y_1 \\ y_2 \end{bmatrix} = \begin{bmatrix} h_{11} & h_{12} & h_{13} & h_{14} \\ h_{21} & h_{22} & h_{23} & h_{24} \end{bmatrix} \begin{bmatrix} 1-c_1 \\ c_1 \\ 1-c_2 \\ c_2 \end{bmatrix} s + \begin{bmatrix} n_1 \\ n_2 \end{bmatrix}. \tag{11}$$

where y_1 and y_2 are the elements of $\mathbf{y}$, n_1 and n_2 are the elements of $\mathbf{n}$, while $h_{i,j}, i = 1, 2, j = 1, 2, 3, 4$ are the elements of the channel matrix $\mathbf{H}$. The mapping rule of GPMod scheme for dual-satellite system is shown in Table I.

B. GPESM System Model

In this subsection, we introduce the ESM concept to the above GPMod system. Let us use a 4×2 dual-polarized MIMO system shown in Fig. 1 (b) for example, where we have a total of $N_t = 2$ transmit antennas and $N_r = 1$ receive antenna. As noted in [23], the number of the active TAs can be one or two in ESM-MIMO. Specifically, when only one TA is active, only a single symbol from the primary signal constellation (such as QPSK) is transmitted, while when two TAs are active, two data symbols from the secondary constellation (such as BPSK) are transmitted simultaneously in parallel. In ESM-MIMO, the transmission with two active TAs leads to a rate increase and the numerical simulation and experimental results have confirmed the BER benefits of ESM compared to other SM-type schemes, e.g., the conventional SM and the generalized SM (GSM).

In the received symbol vector $\mathbf{y} \in \mathbb{C}^{2N_r \times 1}$ at each instant transmission can be expressed as

$$\mathbf{y} = \mathbf{H} \underbrace{\mathbf{Bs}}_{\mathbf{x}} + \mathbf{n}, \tag{12}$$

where $\mathbf{H} \in \mathbb{C}^{2N_r \times 2N_t}$ is dual-polarized MIMO LMS channel matrix, $\mathbf{B}$ is the transmit antenna polarization selection matrix similar to (10), and $\mathbf{s} \in \mathbb{C}^{2N_t \times 1}$ is the transmit ESM symbol vector. For example, for two antennas and QPSK as primary modulation, the transmitted ESM symbol vector is of the form:

$$\mathbf{s} \in \left\{ \begin{bmatrix} C_4 \\ 0 \end{bmatrix}, \begin{bmatrix} 0 \\ C_4 \end{bmatrix}, \begin{bmatrix} B_2^0 \\ B_2^0 \end{bmatrix}, \begin{bmatrix} B_2^1 \\ B_2^1 \end{bmatrix} \right\}, \tag{13}$$

where C_4 denotes the QPSK signal constellation used as primary constellation, and B_2^0 and B_2^1 represent two secondary BPSK constellation given by $B_2^0 \in \{\pm 1\}$ and $B_2^1 \in \{\pm i\}$. In (12), we have the equivalent transmit symbol $\mathbf{x} = \mathbf{Bs}$, whose elements implicitly containing satellite indices, polarization mode and modulated symbols. Moreover, in (12) $\mathbf{n} \in \mathbb{C}^{2N_r \times 1}$ is the zero mean

vector of AWGN with i.i.d. elements and variance of σ^2. The total transmitting power is normalized to one (i.e., $Tr(E[\mathbf{x}^H\mathbf{x}]) = 1$). Similar to (11), the received signal can also be expressed as

$$\begin{bmatrix} y_1 \\ y_2 \end{bmatrix} = \begin{bmatrix} h_{11} & h_{12} & h_{13} & h_{14} \\ h_{21} & h_{22} & h_{23} & h_{24} \end{bmatrix} \mathbf{x} + \begin{bmatrix} n_1 \\ n_2 \end{bmatrix}. \tag{14}$$

Taking the dual-satellite system and QPSK as primary modulation as an example, the transceiver structure of GPESM is shown as Fig. 2.

Note that when two transmit antennas choose the same polarization mode simultaneously for transmission, the cross-polarization interference will be introduced [20]. Thus, these cases are removed in the structure presented. Each symbol contains 5 bits, where the two bits are 4QAM modulation bits and the last three are used to select a combination of ESM symbols containing satellite indices, polarization mode and modulation information. More specifically, the mapping rule of GPESM scheme for dual-satellite system is shown in Table II. Based on the mapping rule given in Table II, the transmitted GPESM symbol vector can be expressed as

C. ML Detection and BER Performance Analysis

Assuming that the system's transmission rate is m bits/s/Hz. At the receiver, the transmitted bit steam is reconstructed by jointly detecting the conventional modulated symbol, the satellite indices and the polarization mode (LHCP or RHCP). Based on the system model given in (12), the optimal 3-D maximum-likelihood detector for the proposed GPESM scheme can be given by

$$\begin{aligned}(u, v)_{\mathrm{ML}} &= \arg\max_{u,v} f_{\mathbf{Y}}(\mathbf{y}|\mathbf{x}, \mathbf{H}) \\ &= \arg\min_{u,v} D(\mathbf{y}, \mathbf{h}_u\mathbf{x}_v),\end{aligned} \tag{15}$$

where $f_{\mathbf{Y}}(\mathbf{y}|\mathbf{x}, \mathbf{H})$ is the conditional probability density function for (12), $\mathbf{x}_v$ is the $v-$th element of the transmitting signal codebook $\mathbb{S}$ for $v = 1, \cdots, 2^m$ and $\mathbf{h}_u$ indicates which column or columns of $\mathbf{H}$ the $\mathbf{x}_v$ corresponds to. For example, in Table II, corresponding to each transmit vector $\mathbf{x} = \mathbf{Bs}$, $\mathbf{h}_u$ can be given by

$$\mathbf{h}_u \in \{[\mathbf{h}_1], [\mathbf{h}_2], [\mathbf{h}_3], [\mathbf{h}_4], [\mathbf{h}_1\mathbf{h}_4], [\mathbf{h}_2\mathbf{h}_3]\}, \quad \text{for } u = 1, \cdots, 6. \tag{16}$$

Moreover, in (15), $D(\mathbf{y}, \mathbf{h}_u\mathbf{x}_v)$ is the minimum squared Euclidian distance between the received vector $\mathbf{y}$ and $\mathbf{h}_u\mathbf{x}_v$, which is given by

$$D(\mathbf{y}, \mathbf{h}_u\mathbf{x}_v) = \|\mathbf{h}_u\mathbf{x}_v\|^2 - 2\mathrm{Re}\left\{\mathbf{y}^H\mathbf{h}_u\mathbf{x}_v\right\}. \tag{17}$$

According to the theory of union bound [35], the BER upper bound of the proposed GPESM is given by

$$P_b \leq \frac{1}{m\ 2^m} \sum_{i=1}^{2^m} \sum_{\substack{j=1 \\ j\neq i}}^{2^m} d(\mathbf{x}_i, \mathbf{x}_j) P(\mathbf{x}_i \to \mathbf{x}_j), \tag{18}$$

where $d(\mathbf{x}_i, \mathbf{x}_j)$ is the Hamming distance between $\mathbf{x}_i$ and $\mathbf{x}_j$. $P(\mathbf{x}_i \to \mathbf{x}_j)$ is the average pairwise error probability (APEP), which is formulated as

$$P(\mathbf{x}_i \to \mathbf{x}_j) = Q\left(\sqrt{\frac{||\mathbf{H}(\mathbf{x}_i - \mathbf{x}_j)||^2}{2N_0}}\right). \tag{19}$$

Considering that $Q(x) = \frac{1}{\pi}\int_0^{\pi/2} \exp(-x^2/2\sin^2\theta)d\theta$, thus

$$P(\mathbf{x}_i \to \mathbf{x}_j) = E\left\{\frac{1}{\pi}\int_0^{\pi/2} \exp(-\frac{||\mathbf{H}(\mathbf{x}_i - \mathbf{x}_j)||^2}{4N_0\sin^2\theta})d\theta\right\}. \tag{20}$$

Using the moment generating function (MGF) approach [20], the unconditional APEP is obtained as in (21), where $k_{i,j}$ is the rank of the distance matrix $(\mathbf{x}_i - \mathbf{x}_j)(\mathbf{x}_i - \mathbf{x}_j)^H$, and the $\lambda_{i,j,1}, \cdots, \lambda_{i,j,k_{i,j}}$ are the no-zero eigenvalues of $(\mathbf{x}_i - \mathbf{x}_j)(\mathbf{x}_i - \mathbf{x}_j)^H$.

Averaging (21) over the channel matrix $\mathbf{H}$, the APEP is obtained as in (22), where K is the Rician factor.

IV. Reliability Improvement Technology For GPESM

To better improve the reliability of the GPESM system, we first apply the optimization-driven AMMD-based PA approach. Then, considering that there may be no perfect channel state information (CSI) in practice and the complexity of the conventional PA approach is too high, we apply the data-driven DNN-based PA approach to the system. As a potential new technology, we also consider to use RIS to assist the GPESM system so as to further enhance the system reliability.

A. AMMD-Based PA Aided GPESM

By adding the power diagonal matrix $\mathbf{P} \in \mathbb{R}^{2N_t \times 2N_t}$, which is given by

$$\begin{aligned}\mathbf{P} &= \mathrm{diag}(\mathbf{p}) \\ &= \begin{bmatrix} p_1 & 0 & \cdots & 0 \\ 0 & p_2 & \cdots & 0 \\ \vdots & \vdots & \ddots & \vdots \\ 0 & 0 & \cdots & p_{2N_t} \end{bmatrix},\end{aligned} \tag{23}$$

where $\mathbf{p} = \{p_1, \cdots, p_q, \cdots, p_{2N_t}\}^T$ represents the power vector at the transmitter and its elements satisfy $\sum_{q=1}^{2N_t} p_q^2 = P_T$ (P_T is the total power constraint), the received signal of the PA-aided GPESM can be re-expressed as

$$\mathbf{y} = \mathbf{HPx} + \mathbf{n}, \tag{24}$$

where $\mathbf{y} \in \mathbb{C}^{2N_r \times 1}$ denotes the received signal vector, $\mathbf{H} \in \mathbb{C}^{2N_r \times 2N_t}$ denotes the channel matrix, $\mathbf{x} \in \mathbb{C}^{2N_t \times 1}$ denotes the transmit GPESM symbol vector, and $\mathbf{n} \in \mathbb{C}^{2N_r \times 1}$ is the zero mean vector of AWGN with i.i.d. elements and variance of σ^2.

At the receiver, the ML detector is formed as

$$\tilde{\mathbf{x}} = \arg\min_{\mathbf{x}\in\mathbb{S}} ||\mathbf{y} - \mathbf{HPx}||^2. \tag{25}$$

By the theory of nearest neighbor bound, the APEP of our PA-aided GPESM is approximated to

$$P(\mathbf{x}_i \to \mathbf{x}_j) \approx \lambda \cdot Q\left(\frac{1}{2N_0} d_{\min}(\mathbf{p})\right), \tag{26}$$

where $Q(\cdot)$ denotes the Q-function, λ is the number of neighbor constellation, and $d_{\min}(\mathbf{p})$ is the minimum squared Euclidian distance between two GPESM symbols $\mathbf{x}_i$ and $\mathbf{x}_j$, which can be obtained by

$$d_{\min}(\mathbf{p}) = \min_{\substack{\forall i,j, \\ i\neq j}} d_{i,j}(\mathbf{p}) = \min_{\substack{\mathbf{x}_i, \mathbf{x}_j \in S, \\ \mathbf{x}_i \neq \mathbf{x}_j}} ||\mathbf{HP}(\mathbf{x}_i - \mathbf{x}_j)||^2. \tag{27}$$

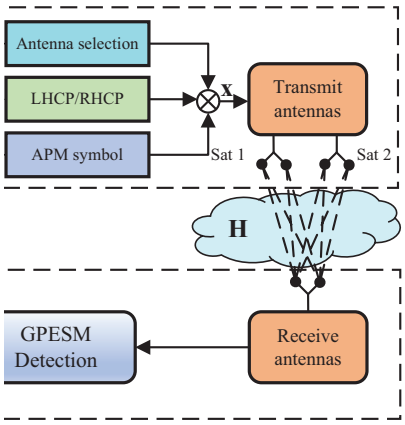

Fig. 2. The transceiver structure of the proposed GPESM scheme.

$$\mathbf{x}=\mathbf{Bs}\in\left\{\begin{bmatrix}C_4\\0\\0\\0\end{bmatrix},\begin{bmatrix}0\\C_4\\0\\0\end{bmatrix},\begin{bmatrix}0\\0\\C_4\\0\end{bmatrix},\begin{bmatrix}0\\0\\0\\C_4\end{bmatrix},\begin{bmatrix}B_2^0\\0\\0\\B_2^0\end{bmatrix},\begin{bmatrix}0\\B_2^0\\B_2^0\\0\end{bmatrix},\begin{bmatrix}B_2^1\\0\\0\\B_2^1\end{bmatrix},\begin{bmatrix}0\\B_2^1\\B_2^1\\0\end{bmatrix}\right\}.$$

TABLE II
GPESM MAPPING RULE FOR 5 BITS/S/HZ TRANSMISSION USING QPSK FOR DUAL POLARIZED DUAL SATELLITE SYSTEMS, WHERE "XX" DENOTES TWO BITS CONVEYED BY PSK SYMBOLS.

Transmit bits	Satellite1-LHCP	Satellite1-RHCP	Satellite2-LHCP	Satellite2-RHCP
000XX	C_4	0	0	0
001XX	0	C_4	0	0
010XX	0	0	C_4	0
011XX	0	0	0	C_4
100XX	B_2^0	0	0	B_2^0
101XX	0	B_2^0	B_2^0	0
110XX	B_2^1	0	0	B_2^1
111XX	0	B_2^1	B_2^1	0

Since the error bits mainly occur in the nearest neighbors, the maximization of $d_{\min}(\mathbf{p})$ is capable of reducing the probability of error events, especially at high signal-to-noise ratio (SNR) regions. Based on this observation, thus we can formulated the PA algorithm to improve the BER of the proposed GPESM as the following maximum minimum distance (MMD) problem

$$\begin{aligned}\max_{\mathbf{p}}\quad & d_{\min}(\mathbf{p}),\\ s.t.\quad & ||\mathbf{p}||^2\le P_T.\end{aligned}\tag{28}$$

To solve this optimization problem, we can first transform the objective function $d_{i,j}(\mathbf{p})$ to a simple form, given by

$$\begin{aligned}d_{i,j}(\mathbf{p})&=\|\mathbf{HP}(\mathbf{x}_i-\mathbf{x}_j)\|^2\\&=(\mathbf{x}_i-\mathbf{x}_j)^H\mathbf{P}^H\mathbf{H}^H\mathbf{HP}(\mathbf{x}_i-\mathbf{x}_j)\\&=Tr(\mathbf{P}^H\mathbf{H}^H\mathbf{HP}(\mathbf{x}_i-\mathbf{x}_j)(\mathbf{x}_i-\mathbf{x}_j)^H)\\&=\mathbf{p}^H\left(\mathbf{H}^H\mathbf{H}\odot\left((\mathbf{x}_i-\mathbf{x}_j)(\mathbf{x}_i-\mathbf{x}_j)^H\right)\right)\mathbf{p}\\&=\mathbf{p}^H\mathbf{R}_{ij}\mathbf{p},\end{aligned}\tag{29}$$

where $\mathbf{R}_{ij}=\mathbf{H}^H\mathbf{H}\odot\left[(\mathbf{x}_i-\mathbf{x}_j)(\mathbf{x}_i-\mathbf{x}_j)^H\right]$. Based on (29), the challenging optimization problem (28) can be

$$P(\mathbf{x}_i\to\mathbf{x}_j)=\frac{1}{\pi}\int_0^{\pi/2}\left(\frac{1}{1+\frac{\lambda_{i,j,1}}{4N_0\sin^2\theta}}\right)^{2N_r}\times\left(\frac{1}{1+\frac{\lambda_{i,j,2}}{4N_0\sin^2\theta}}\right)^{2N_r}\times\cdots\times\left(\frac{1}{1+\frac{\lambda_{i,j,k_{i,j}}}{4N_0\sin^2\theta}}\right)^{2N_r}d\theta,\tag{21}$$

$$\begin{aligned}P(\mathbf{x}_i\to\mathbf{x}_j)=\frac{1}{\pi}\int_0^{\pi/2}&\left\{\frac{(1+K)\sin^2\theta}{(1+K)\sin^2\theta+\lambda_{i,j,1}}\exp[-\frac{K\lambda_{i,j,1}}{(1+K)\sin^2\theta+\lambda_{i,j,1}}]\right\}^{2N_r}\times\\&\left\{\frac{(1+K)\sin^2\theta}{(1+K)\sin^2\theta+\lambda_{i,j,2}}\exp[-\frac{K\lambda_{i,j,2}}{(1+K)\sin^2\theta+\lambda_{i,j,2}}]\right\}^{2N_r}\times\cdots\\&\times\left\{\frac{(1+K)\sin^2\theta}{(1+K)\sin^2\theta+\lambda_{i,j,k_{i,j}}}\exp\left[-\frac{K\lambda_{i,j,k_{i,j}}}{(1+K)\sin^2\theta+\lambda_{i,j,k_{i,j}}}\right]\right\}^{2N_r}d\theta.\end{aligned}\tag{22}$$

Algorithm 1 Proposed AMMD-based PA Algorithm

Input: Initialize $\mathbf{p}_\alpha = \mathbf{p}_0 = \mathbf{I}_{2N_t\times 1}$, $\varepsilon = 0.01$, $k = 1$
Output: $\mathbf{p}_{k+1}$
Step1: $\mathbf{p}_k = \mathbf{p}_\alpha$;
Step2: Solve the problem by the interior point method to get $\mathbf{p}_{k+1}$;
Step3: $\mathbf{p}_k = \mathbf{p}_{k+1}$;
Step4: $k = k + 1$.
Repeat Step2 to **Step4**
Until $\|\mathbf{p}_{k+1} - \mathbf{p}_k\| \le \varepsilon$
Return result

simplified to

$$\begin{aligned} \max_{\mathbf{p}} \min \ & \mathbf{p}^H\mathbf{R}_{ij}\mathbf{p} \quad \forall i,j,i\neq j \\ s.t. \ & \|\mathbf{p}\|^2 \le P_T. \end{aligned} \tag{30}$$

To solve this QCQP problem given in (30), we can introduce the auxiliary scalar variable t and the AMMD problem is finally given by [33]

$$\begin{aligned} \max_{\mathbf{p}} \ & t \\ s.t. \ & \mathrm{Re}\left\{2\mathbf{p}_k^H\mathbf{R}_{ij}\mathbf{p} - \mathbf{p}_k^H\mathbf{R}_{ij}\mathbf{p}_k\right\} \ge t, \quad \forall i,j,i\neq j \\ & ||\mathbf{p}||^2 \le P_T. \end{aligned} \tag{31}$$

Since $\mathrm{Re}\left\{2\mathbf{p}_k^H\mathbf{R}_{ij}\mathbf{p} - \mathbf{p}_k^H\mathbf{R}_{ij}\mathbf{p}_k\right\}$ is an affine function of $\mathbf{p}$, (31) is a convex problem. Therefore, the AMMD problem can be solved by classic convex solvers. The procedure of the AMMD-based PA method is detailed in Algorithm 1.

B. DNN-Based PA Aided GPESM

In this section, compared to the above optimization-driven PA algorithm, we introduce the concept of machine learning to carry out the PA matrix optimization, since it have been viewed as a key enabler for beyond 5G communications. Specifically, a feed-forward DNN based multi-label classifier is proposed for PA-aided GPESM, since DNN is an important branch in machine learning and is a promising and powerful tool for optimization.

Unlike the AMMD method, we need to generate a PA codebook beforehand in DNN-based PA algorithm, which is available to both the transmitter and receiver before transmission. Let P_p be the codebook for the DNN-based PA-aided GPESM scheme, which is given by

$$P_p = \{\mathbf{P}_1, \cdots, \mathbf{P}_q, \cdots, \mathbf{P}_Q\}, \tag{32}$$

where Q is the total number of selection candidates. Similar to the AMMD method, the optimization problem is also maximum the minimum squared Euclidian distance between two GPESM symbols.

Based on (32) and (27), the PA matrix optimization problem can be considered as a classification problem, which can be efficiently solved by using DNN architecture. To be specific, in general, we can consider to steps in DNN for this problem, namely the training step and the learning step. The specific procedures of the training step include the training data generation, the feature vector extraction, the key performance indicator (KPI) design and labeling. Next, we briefly introduce these procedures as follows:

1) *Training Data Generation*: In DNN, we can directly use the channel matrices to train the neural network nodes. For this propose, a set of training data can be generated by M random channel matrices $\mathbf{H}^m, m = 1, \cdots, M$ based on the channel model given in (1)-(7), i.e.,
$$\mathbb{H} = \left\{\mathbf{H}^1, \mathbf{H}^2, \cdots, \mathbf{H}^m, \cdots, \mathbf{H}^M\right\}. \tag{33}$$
2) *Feature Vector Extraction*: For achieving better training performance and fast convergence, we joint consider the modulus (i.e., $(\mathbf{h}_i^m)^H\mathbf{h}_i^m, i = 1\cdots, N_t$) and correlations (i.e., $(\mathbf{h}_i^m)^H\mathbf{h}_j^m, i \neq j$) of channel vectors, which determine the BER performance of the conventional PSK/QAM bits and the error performance of the bits mapped to the satellite indices and the polarization mode, respectively. Specifically, we consider the following feature vector
$$\mathbf{f} = \left[|(\mathbf{h}_1^m)^H\mathbf{h}_1^m|, \cdots, |(\mathbf{h}_i^m)^H\mathbf{h}_j^m|, |(\mathbf{h}_{2N_t}^m)^H\mathbf{h}_{2N_t}^m|\right], \tag{34}$$
where $\mathbf{h}_i, i = 1, \cdots, N_t$ is the i-th column of $\mathbf{H}$. to avoid the bias problem in the learning phase, the feature vector of (34) can be further normalized to,
$$\tilde{f}(n) = (f(n) - E[f])/(\max(f) - \min(f)), \tag{35}$$
where $f(n)$ is the n-th element of the feature vector $\mathbf{f}$.
3) *KPI Design*: Similar to the PA algorithm introduced in Section IV-A, we adopt the maximum value of $d_{\min}$ in (27) all possible power candidates given in (32) as the KPI, in order to improve the attainable BER performance. Based on the KPI, we can classify the training samples, i.e., the generated training channel matrices, to different sets.
4) *Labeling*: In our design, each power candidate has its index number. The labels for training matrices can be calculated by following steps:
Step 1: Input the m-th training sample $\mathbf{H}^m$, and compute the KPI $d_{\min}$ for all possible power candidates $\mathbf{P}_p, p \in \{1, \cdots, Q\}$.
Step 2: Obtain the power candidate $\mathbf{P}_{q^*}$ with the maximum $d_{\min}$ and its index label $q^*, q^* \in \{1, \cdots, Q\}$. The index label of the final obtained optimal power candidate is converted to one-hot code, denoted as $\mathbf{r}_c$.
Step 3: Repeat Steps 1 and Steps 2 until all training samples' labels are found.

We consider DNN as a "black box" and utilize it to explore the nonlinear mapping relationship between the feature vector $\mathbf{f}$ and one-hot code $\mathbf{r}_c$. Once all the training data is ready, assume that we have L layers in the feed-forward DNN and the mapping relationship of the DNN layers is given by

$$\begin{aligned} \mathbf{r}_c^L = F_{L-1}(F_{L-2}(\cdots(F_1(\mathbf{r}_c^0;\boldsymbol{\theta}^1),\cdots);\boldsymbol{\theta}^{L-2});\boldsymbol{\theta}^{L-1}), \\ l = 1, \cdots, L, \end{aligned} \tag{36}$$

where $F_l(\mathbf{r}_c^{l-1};\boldsymbol{\theta}^l) = \Delta(\mathbf{W}^l\mathbf{r}_c^{l-1} + \mathbf{b}^l), \quad l = 1, \cdots, L$, and $\mathbf{r}_c^L$ is the output vector through L iterative precessing steps. In this paper, we employ the fully connected layers and $\boldsymbol{\theta}^l = \{\mathbf{W}^l, \mathbf{b}^l\}$, $\mathbf{W}^l$ and $\mathbf{b}^l$ are the weight and bias parameter vectors of l-th layer, and $\Delta(\cdot)$ is an activation function. In our design, we consider stochastic gradient decent (SGD) as the optimization method and categorical cross-entropy as the loss function. The procedure of the

Algorithm 2 Proposed DNN-based Classification PA Algorithm

Input: Training set: $\mathbf{f}_{\text{train}}$ and $\mathbf{r}_{c-\text{train}}$, testing set: $\mathbf{f}_{\text{test}}$ and $\mathbf{r}_{c-\text{test}}$, prediction set: $\mathbf{f}_{\text{pred}}$, power candidates set: $\mathbf{P}_p$, $i = 1$, $epochs = 128$, accuracy threshold: $\tau = 70\%$

Output: $\mathbf{P}_{q^*-\text{pred}}$

Step1: Enter $\mathbf{f}_{\text{train}}$ and $\mathbf{r}_{c-\text{train}}$ into the initial DNN network;

Step2: For $1 \leq i \leq epochs$, update DNN network parameters $\boldsymbol{\theta}_k$ using SGD optimization method and set $i = i + 1$;

Step3: Get testing accuracy τ_c by entering $\mathbf{f}_{\text{test}}$ and $\mathbf{r}_{c-\text{test}}$ into DNN network;

Step4: If $\tau_c \leq \tau$, change the number of nodes and layers of the DNN network, then go to **Step2**; Others go to **Step5**;

Step5: Enter $\mathbf{f}_{\text{pred}}$ into the DNN network to get $\mathbf{r}_{c-\text{pred}}$;

Step6: Get $\mathbf{P}_{q^*-\text{pred}}$ according to power candidates set $\mathbf{P}_p$ and $\mathbf{r}_{c-\text{pred}}$.

Return result

Algorithm 3 Proposed DNN-based Regression PA Algorithm

Input: Training set: $\mathbf{f}_{\text{train}}$ and $\mathbf{r}_{r-\text{train}}$, prediction set: $\mathbf{f}_{\text{pred}}$, $i = 1$, $epochs = 128$

Output: $\mathbf{P}_{r-\text{pred}}$

Step1: Enter $\mathbf{f}_{\text{train}}$ and $\mathbf{r}_{r-\text{train}}$ into the initial DNN network;

Step2: For $1 \leq i \leq epochs$, update DNN network parameters $\boldsymbol{\theta}_k$ using Adam optimization method and set $i = i + 1$;

Step3: Enter $\mathbf{f}_{\text{pred}}$ into the DNN network to get $\mathbf{r}_{r-\text{pred}}$;

Step4: Get $\mathbf{P}_{r-\text{pred}}$ according to $\mathbf{r}_{r-\text{pred}}$.

Return result

DNN-based classification PA method is given in Algorithm 2.

In addition to this, the power allocation problem can also be considered as a regression problem, due to the continuity nature of the channel state information and the allocated power. The difference between the regression problem and the classification problem is that the training output vector $\mathbf{r}_r$ in the regression problem is the power set derived by iterating using Algorithm 1. Suppose we have obtained the power vector $\mathbf{p}_r = \{p_1, \cdots, p_q, \cdots, p_{2N_t}\}^T$, the first $2N_t$ elements of training output vector $\mathbf{r}_r$ are $2N_t$ power values in $\mathbf{p}_r$. Besides, $\mathbf{r}_r$ also contains a sum of $2N_t$ power values to satisfy the power constraint and increase the estimation accuracy [36]. Therefore, $\mathbf{r}_r$ is a vector of $2N_t + 1$ columns. The input data of DNN in regression problem is the same as that of classification problem.

Assuming that we also have L layers in the feed-forward DNN, the mapping relationship of the DNN layers in regression problem is similar to (36). We consider mean square error as the loss function and Adam optimizer. The procedure of the DNN-based regression PA method is given in Algorithm 3.

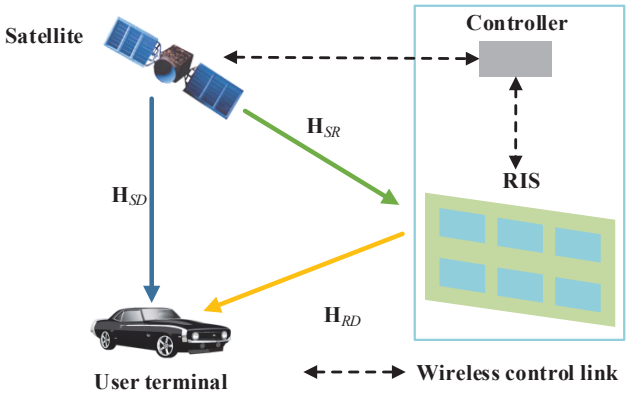

Fig. 3. The proposed RIS-assisted GPESM scheme.

C. RIS-Assisted GPESM System Model

Compared to PA algorithms, recent studies have shown that reconfigurable intelligent surfaces can provide attractive performance improvements under various application scenarios. In this paper, in order to achieve an enhanced spatial diversity gain, we consider to apply a reconfigurable intelligent surface to the proposed GPESM system as a relay to assist in transmitting information. To be specific, we propose a RIS-assisted GPESM system depicted in Fig. 3, where the signal is sent by satellite and assisted by RIS to mobile users. The number of units in each RIS is set to be N_s. Although the current hardware designs only contain discrete phase shifters [29], RIS with low resolution and few units may appear in the future, which is suitable for LMS scenarios. Therefore, we still assume that each reflecting unit can reconstruct the phase and amplitude of the incident signal via a software controller. According to [30], RIS units are taken as a certain number of discrete phase and module values. We denote the coefficients of the RIS reflection unit by a vector, which is given by

$$\mathbf{v} = [\mu_1 e^{j\theta_1}, \mu_2 e^{j\theta_2}, \ \cdots \ , \mu_N e^{j\theta_N}]^{\mathrm{T}}, \tag{37}$$

where μ_k and θ_k are the reflection amplitude and phase of the reflecting unit on the RIS, respectively [29]. Suppose that

$$\mathbb{U} = \left\{0, \frac{1}{2^{Q_\alpha} - 1}, \frac{2}{2^{Q_\alpha} - 1}, \ \cdots \ , 1\right\}, \tag{38}$$

$$\mathbb{G} = \left\{0, \frac{2\pi}{2^{Q_\theta}}, \ \cdots \ , \frac{2\pi(2^{Q_\theta} - 1)}{2^{Q_\theta}}\right\}, \tag{39}$$

where $\mathbb{U}$ is the set of reflection amplitudes and $\mathbb{G}$ is the set of reflection phases. 2^{Q_α} and 2^{Q_θ} denote the number of legitimate reflection amplitudes and phases in each RIS unit, respectively. Hence,

$$\mathbf{v}[n] \in \Phi = \left\{\mu_n e^{j\theta_n} | \mu_n \in \mathbb{U}, \theta_n \in \mathbb{G}\right\}, \quad n = 1, \cdots, N_s. \tag{40}$$

Based on the proposed GPESM system model given in Section III-B, the received symbol vector $\mathbf{y} \in \mathbb{C}^{2N_r \times 1}$ of the RIS-assisted GPESM can be formulated as

$$\mathbf{y} = (\mathbf{H}_{SD} + \mathbf{H}_{RD}\mathbf{V}\mathbf{H}_{SR})\mathbf{x} + \mathbf{n}_1, \tag{41}$$

where $\mathbf{H}_{SD} \in \mathbb{C}^{2N_r \times 2N_t}$, $\mathbf{H}_{RD} \in \mathbb{C}^{2N_r \times N_s}$ and $\mathbf{H}_{SR} \in \mathbb{C}^{N_s \times 2N_t}$ denote the MIMO LMS channel matrices between satellite and UT, RIS and UT, satellite and RIS, respectively. $\mathbf{V} = \text{diag}(\mathbf{v})$ denotes the diagonal matrix of $\mathbf{v}$.

$\mathbf{x} \in \mathbb{C}^{2N_t \times 1}$ is the GPESM symbol vector. $\mathbf{n}_1 \in \mathbb{C}^{2N_r \times 1}$ is the zero mean vector of AWGN with i.i.d. elements and variance of σ^2.

In this paper, we consider exhaustively searching all the values of $\mathbf{v}$, and then find an optimal $\mathbf{v}^*$, which equals to the following problem

$$\max_{\mathbf{v}^*} \min_{i \neq j} \quad \|(\mathbf{H}_{SD} + \mathbf{H}_{RD}\mathbf{V}\mathbf{H}_{SR})(\mathbf{x}_i - \mathbf{x}_j)\|^2, \tag{42}$$

where $\mathbf{x}_k$ is the $k-$th element of the transmit GPESM signal codebook $\mathbb{S}$ for $k = 1, \cdots, 2^m$.

At the receiver, the ML detection is similar to (15), which is formulated as

$$\hat{\mathbf{x}} = \arg\min_{\mathbf{x} \in \mathbb{S}} \quad \|\mathbf{y} - (\mathbf{H}_{SD} + \mathbf{H}_{RD}\mathbf{V}\mathbf{H}_{SR})\mathbf{x}\|^2. \tag{43}$$

Moreover, for the RIS-assisted GPESM system given in (41), we can also employ the PA algorithm for achieving further performance improvement and the detector can be given by changing (43) to

$$\hat{\mathbf{x}} = \arg\min_{\mathbf{x} \in \mathbb{S}} \quad \|\mathbf{y} - (\mathbf{H}_{SD} + \mathbf{H}_{RD}\mathbf{V}\mathbf{H}_{SR})\mathbf{P}\mathbf{x}\|^2, \tag{44}$$

where $\mathbf{P} = \text{diag}(\mathbf{p}) = \text{diag}(\{p_1, \cdots, p_q, \cdots, p_{2N_t}\}^T)$.

According to (44), the conditional PEP is obtained as

$$\begin{aligned} &P(\mathbf{x}_i \to \mathbf{x}_j|\mathbf{H}) \\ =&Q\left(\sqrt{\frac{||(\mathbf{H}_{SD} + \mathbf{H}_{RD}\mathbf{V}\mathbf{H}_{SR})\mathbf{P}(\mathbf{x}_i - \mathbf{x}_j)||^2}{2N_0}}\right). \end{aligned} \tag{45}$$

From (45), it can be observed that the APEP of this system depends on the design of $\mathbf{v}$ and $\mathbf{P}$. Therefore, our problem is translated to the design of the reflection coefficients value of the RIS units and the precoding power matrix to minimize the APEP of the system. By maximizing minimum Euclidean distance criterion for the design of $\mathbf{v}$ and $\mathbf{P}$, our optimization problem can be expressed as:

$$\begin{aligned} \max_{\mathbf{v},\mathbf{P}} \min_{\forall i \neq j} &\left\{||(\mathbf{H}_{SD} + \mathbf{H}_{RD}\mathbf{V}\mathbf{H}_{SR})\mathbf{P}(\mathbf{x}_i - \mathbf{x}_j)||^2\right\} \\ s.t. \quad &||\mathbf{p}||^2 \leq P_T, \\ &\mathbf{v}[n] \in \Phi, \quad n = 1, \cdots, N_S. \end{aligned} \tag{46}$$

For the sake of simplicity, we can employ the iteration algorithm and our proposed PA algorithms to solve the problem of (46). Specifically, let's assume that we fix $\mathbf{v}$ by using (42) in an iteration step and then update $\mathbf{P}$. Thus, the optimization problem in (46) is reduced to the following question:

$$\begin{aligned} \max_{\mathbf{P}} \min_{\forall i \neq j} &\left\{||(\mathbf{H}_{SD} + \mathbf{H}_{RD}\mathbf{V}\mathbf{H}_{SR})\mathbf{P}(\mathbf{x}_i - \mathbf{x}_j)||^2\right\} \\ s.t. \quad &||\mathbf{p}||^2 \leq P_T, \end{aligned} \tag{47}$$

It is noted that the above problem in (47) is identical to that in (28). Later we can use the AMMD or DNN method to get $\mathbf{P}$. The procedure of the PA algorithm for RIS-assisted GPESM system is given in Algorithm 3.

D. Complexity Comparison For Different Optimization Algorithms For GPESM

By recalling the complexity order for solving the MMD convex problem given in [33], the complexity order of the AMMD-based PA algorithm is $O(8N_t^2M^2N_r)+O(16N_t^4M^4)$. By contrast, based on the model given in Section IV-B, most of the computation of the DNN-based PA algorithm is consumed in the generation of the training set. In particular, the training set of the classification PA algorithm needs to exhaustively search the pre-defined power sets under all channels to find the optimal power set labels, and the training set of the regression PA algorithm needs to use the AMMD-based PA algorithm to derive the optimal assigned power under all channels. If we assume that the training sets have been generated, then the complexity order of the DNN-based PA algorithm will be greatly reduced to $O(64N_t^4 + 4N_t^2)$ [25]. For RIS-assisted GPESM scheme, there are $2^{Q_a+Q_\theta}$ possible values for the RIS unit and $(2^{Q_a+Q_\theta})^{N_s}$ possible candidate sets for RIS with N_s units. Therefore, the complexity order of the RIS-assisted GPESM is $O(4(2^{Q_a+Q_\theta})^{N_s}N_t^2M^2)$.

In summary, the RIS method requires an exhaustive search over $(2^{Q_a+Q_\theta})^{N_s}$ candidate sets, and its complexity order increases exponentially with increasing number of N_s and quantization levels. The AMMD approach introduces additional complexity during the computation of the convex optimization problem, while the DNN method is quite simple compared to it, when the training sets are all generated. Table III is the complexity comparison for different optimization algorithms for GPESM.

Algorithm 4 Proposed PA Algorithm for RIS-assisted GPESM system

Input: Channel matrix $\mathbf{H}_{SD}$, $\mathbf{H}_{RD}$, $\mathbf{H}_{SR}$
Output: $\mathbf{P}$
Step1: Fix $\mathbf{v}$ by using (42);
Step2: Use **Algorithm 1** to solve problem (47) or use **Algorithm 2** or **3** to get $\mathbf{P}$;
Return result

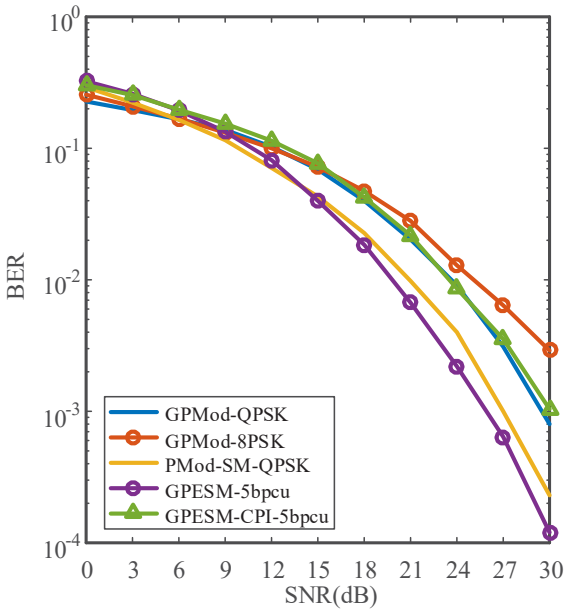

Fig. 4. The BER performance comparison of the proposed GPESM and GPMod schemes with different CPI.

V. Simulation Results And Discussion

In this section, we apply the the LMS channel parameters in [14]. For GPESM and GPMod, the number of

TABLE III
COMPARISON OF COMPLEXITY ORDERS OF DIFFERENT OPTIMIZATION ALGORITHMS FOR PA-GPESM CHEMES

PA-GPESM schemes	Complexity order	Configuration (4×2, QPSK, $Q_\alpha = 2$, $Q_\theta = 2$, $N_s = 3$)
Proposed AMMD-based PA-GPESM	$O(8N_t^2M^2N_r)$+$O(16N_t^4M^4)$	66048
Proposed DNN-based PA-GPESM	$O(64N_t^4 + 4N_t^2)$	1088
Proposed RIS-assisted GPESM	$O(4(2^{Q_\alpha+Q_\theta})^{N_s}N_t^2M^2)$	1048576

TABLE IV
LAYOUTS OF THE DNN STRUCTURES

	Classification		Regression	
	Size	Activation function	Size	Activation function
Input	16	Relu	16	-
Layer1(Dense)	32	Relu	32	Relu
Layer2(Dense)	32	Relu	32	Relu
Layer3(Dense)	64	Relu	64	Relu
Layer4(Dense)	32	Relu	32	Relu
Layer5(Dense)	32	Relu	16	Relu
Layer6(Dense)	16	Softmax	5	Relu

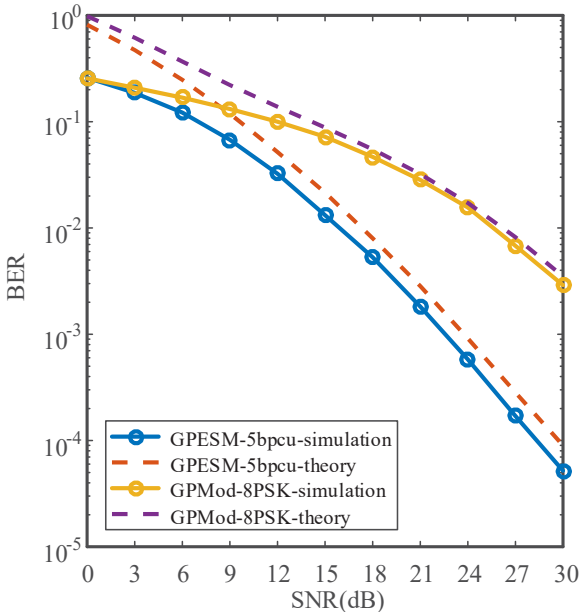

Fig. 5. Simulation and theoretical performance comparison of the proposed GPESM and GPMod schemes.

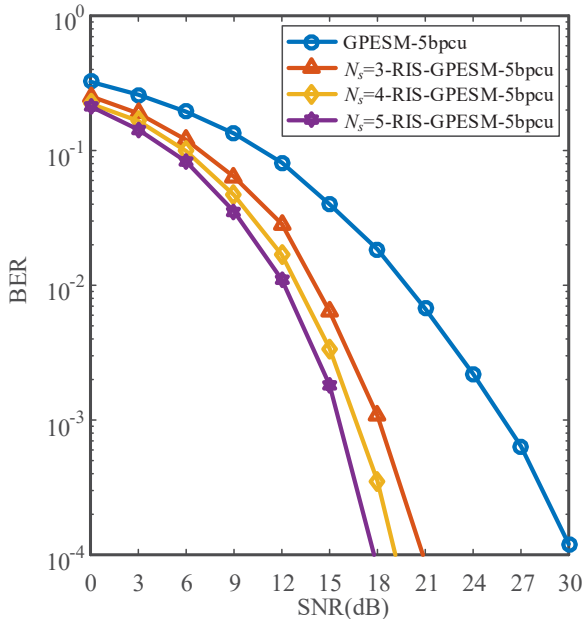

Fig. 6. BER performance comparison of the proposed RIS-assisted GPESM scheme with different numbers of reflection units.

training data sets is 80000, the number of testing data sets is 20000 and the number of power candidates is 16. Layouts of the DNN structures are shown in Table IV. Due to the performance of the simulation computer and time constraints, we generate 1000 RIS channel matrices. The number of realizations is 2×10^6 at each SNR. For the sake of discussion, this paper only discusses the good state cases in suburban areas for 4×2 dual polarized LMS MIMO channel with dual satellites. Here, for comparison, serval conventional schemes, such as the PMod-SM of [19] and the GPMod of [20] are utilized as the benchmarkers.

In order to show that the proposed GPESM system is resilient to CPI, we first compare the BER performance of systems with different CPI in Fig. 4. First, the PMod-SM with QPSK modulation in the Fig. 4 refers to the structure in Table II where only the first four combinations are selected. The transmit antenna activates only one polarization at each moment to transmit the signal, thus completely eliminating the CPI. We can see that PMod-SM with QPSK modulation has a 3 dB BER performance gain than the GPMod with QPSK modulation. Then, as shown in the Fig. 4, the proposed GPESM with 5 bpcu achieves nearly 6 dB gain over GPMod with 8PSK at BER $= 10^{-2}$, which demonstrates that the proposed GPESM scheme not only mitigates the impact of CPI, but also achieves the benefits of multiple constellation ensembles. To further confirm the performance of the proposed GPESM scheme, we also compare it with the GPESM-CPI scheme, which refers to the GPESM scheme with full CPI by replacing the first four combinations in Table II with combinations that simultaneously activate the same polarization in both satellites using multiple signal constellations. In Fig. 4, the proposed GPESM scheme still achieves 5 dB BER gain over the GPESM-CPI scheme in the high SNR case. Moreover, the GPESM-CPI with 5bpcu has almost the same performance as GPMod with QPSK modulation, which proves the powerful benefit of using multiple constellations on the other hand.

Fig. 5 provides the simulated and theoretical BER performance curves for the GPESM and GPMod schemes.

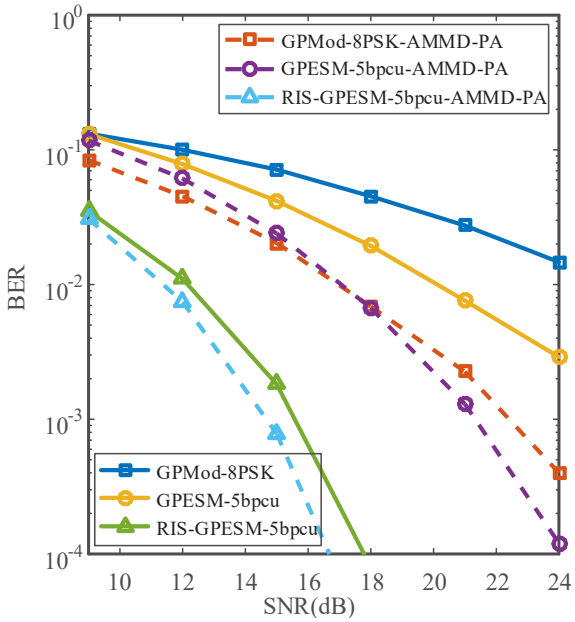

Fig. 7. BER performance comparison of the GPMod and GPESM schemes with AMMD-based PA algorithm.

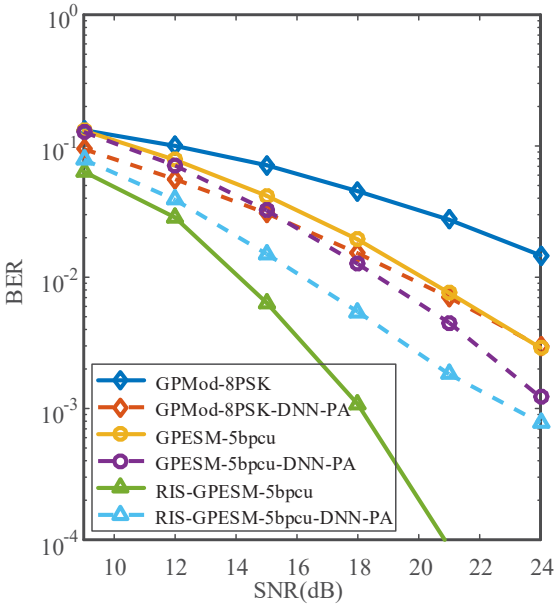

Fig. 9. BER performance comparison of the GPMod and GPESM schemes with DNN-based PA algorithm.

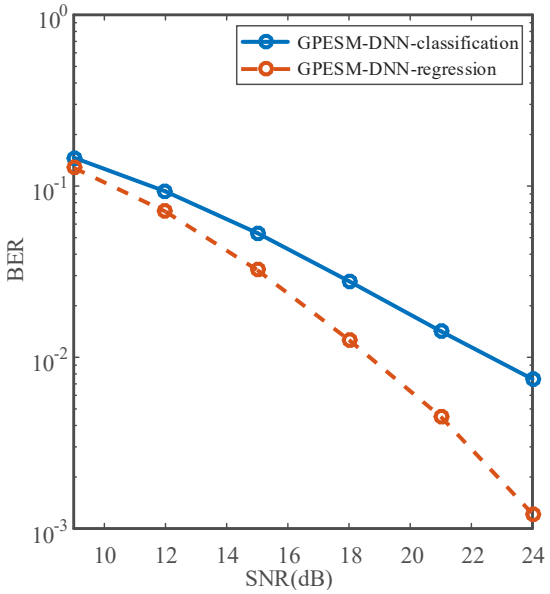

Fig. 8. BER performance comparison of the GPESM scheme with DNN-based classification PA algorithm and regression PA algorithm.

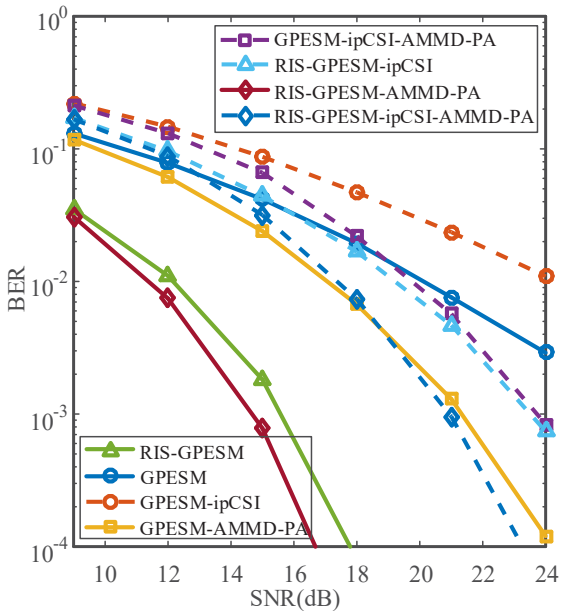

Fig. 10. BER performance comparison of the GPMod and GPESM schemes with AMMD-based PA algorithm in the presence of CSI errors.

As shown in the Fig. 5, the theoretical line becomes closer to the simulation line as the SNR increases.

In Fig. 6, we compare the BER performance of RIS-assisted GPESM schemes with different numbers of units. For the sake of simplification, assume that RIS has perfect known CSI for all channels and $Q_\alpha = 2$, $Q_\theta = 2$. All RIS-assisted GPESM systems have substantial BER performance gains compared to the standard GPESM. In particular, the RIS-assisted GPESM with $N_s = 5$ has a BER performance gain of more than 10 dB when SNR = 15 dB or more. From Fig. 6, it can be learned that as the number of N_s increases, the better the BER performance of the system will be.

To further enhance the reliability of the system, in Fig. 7, we apply the AMMD-based PA algorithm to the GPMod, GPESM and RIS-assisted GPESM systems. Assume that CSI is perfectly known at the transmitter and $N_s = 5$. We can observe BER performance improvements in all three systems after applying the AMMD-based PA algorithm. In particular, GPMod with 8PSK modulation achieves a gain of 6 dB at SNR = 12 dB. Overall, after applying the AMMD-based PA algorithm, RIS-assisted GPESM performs much better than GPESM and GPMod, followed by GPESM and finally GPMod.

To explore whether classification or regression is more appropriate when utilizing DNN for power allocation, we compare the BER performance of the two method in the GPESM with 5bpcu system in Fig. 8. From Fig. 8, it can be found that the regression method consistently has a better BER performance than the classification method for SNR = 9 dB or more. At BER = 10^{-2}, the regression

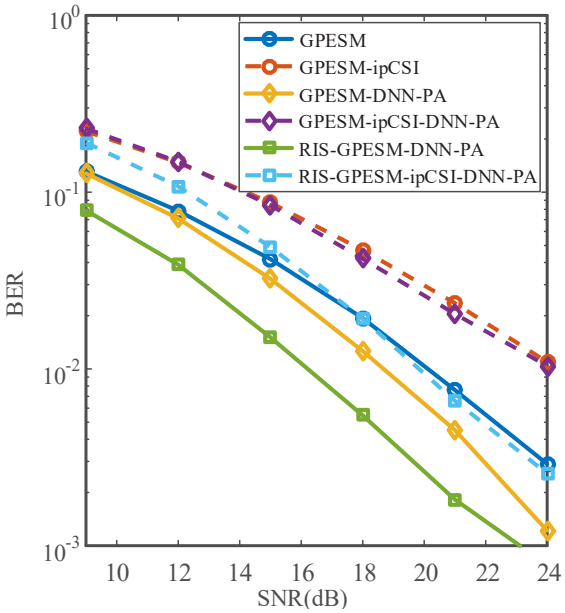

Fig. 11. BER performance comparison of the GPMod and GPESM schemes with DNN-based PA algorithm in the presence of CSI errors.

method has a 5 dB higher performance gain than the classification method. We find that the accuracy of the classification method is not good when a large number of power combinations are preset. No matter how to adjust the structure of DNN during simulation, the accuracy of multi-category classification is bad, even less than 60%. Therefore, the classification method of DNN cannot be well applied in GPESM power allocation system. The advantages of the regression method are reflected in the fact that the training set is generated by the AMMD method, which has a higher KPI compared to the classification method. Secondly, the regression method can better reflect the continuity of channel information and allocated power, and better reflect the mapping relationship between the two. The DNN power allocation methods considered in the subsequent articles are all regression method.

Fig. 9 shows a comparison of the BER performance of GPMod, GPESM and RIS-assisted GPESM with the DNN-based PA algorithm applied. Assume that CSI is perfectly known at the transmitter and $N_s = 3$. Under this algorithm, the crossover between GPMod and GPESM schemes still occurs and GPESM can highlight its own performance advantages for SNR $=$ 15 dB or more. Both systems perform better than the standard GPESM and GPMod systems. However, the performance of RIS-assisted GPESM with DNN-based PA is not as good as RIS-assisted GPESM itself. It can be seen that the power allocation with DNN will instead have a negative impact on the RIS-assisted GPESM, which is a high precision system. It is worth noting that our proposed RIS-assisted GPESM with DNN-based PA still has better BER performance than the other two systems with DNN-based PA.

Fig. 10 and Fig. 11 show the BER performance of various GPESM schemes in the case of Gaussian-distributed CSI errors, which is modelled as the zero mean vector of AWGN with i.i.d. elements and variance of σ_{err}^2. Assume that the value of σ_{err}^2 decreases with SNR increasing and $N_s = 5$ in Fig. 10 and $N_s = 3$ in Fig. 11. From Fig. 10 and Fig. 11, we can observe that the BER performance of the RIS-assisted GPESM schemes drops very sharply compared to the GPESM schemes in the presence of CSI errors. We can also learn that RIS is very sensitive to CSI. In the case of SNR $\leq$ 15 dB, the RIS-assisted GPESM system does not have a great BER performance advantage, which will instead cause a large computing overhead. With SNR $\geq$ 20 dB, the RIS-assisted GPESM system still performs well compared to other standard systems due to the reduced CSI errors. In particular, the RIS-assisted GPESM system has a similar performance to the AMMD power allocation method in the presence of CSI errors in Fig. 10. Considering that RIS has a higher overhead than AMMD power allocation method, it is more suitable to apply AMMD power allocation method directly in this case. The difference in performance between the GPESM system and the GPESM system with the addition of the DNN power allocation method is also not significant in the presence of CSI errors in Fig. 11.

VI. Conclusion

In this paper, a novel satellite scheme called GPESM has been proposed for MIMO satellite communication systems. Our simulation results show that GPESM or RIS-assisted GPESM enjoys better BER performance than the conventional GPMod scheme. In addition, we have also proposed two PA strategies for GPESM, namely the AMMD-based PA method and DNN-based PA method, where AMMD-based PA method enjoys the best BER performance with high complexity and DNN-based PA method is suboptimal with low complexity. These two PA strategies have led to improved BER performance compared to that of GPESM. It is also noted that RIS-assisted GPESM is able to meet or exceed the BER performance of PA-based GPESM systems, thus demonstrating the reliability that RIS can provide to the system. Considering both the BER versus complexity trends, we conclude that the proposed RIS-assisted GPESM with DNN-based PA method provides an improved BER performance at a modest complexity cost. In addition to this, we will investigate low-complexity RIS algorithms in our subsequent work. Our future work will also focus on more realistic channels and attempt to combine the proposed scheme with a multi-UAVs system.

References

[1] L. Zhang, Y. Liang, and D. Niyato, "6G visions: Mobile ultra-broadband, super internet-of-things, and artificial intelligence," *China Commun.*, vol. 16, no. 8, pp. 1-14, Aug. 2019.

[2] M. Giordani and M. Zorzi, "Satellite communication at millimeter waves: A key enabler of the 6G era," in *IEEE International Conference on Computing, Networking and Communications (ICNC)*, Big Island, HI, USA, Feb. 2020, pp. 383-388.

[3] T. Huang, W. Yang, J. Wu, J. Ma, X. Zhang, and D. Zhang, "A survey on green 6G network: Architecture and technologies," *IEEE Access*, vol. 7, pp. 175758-175768, Dec. 2019.

[4] P. Chini, G.Giambene, and S. Kota, "A survey on mobile satellite systems," *Int. J. Commun. Syst. Network.*, vol. 28, no. 1, pp. 29-57, Jan. 2010.

[5] J. Wei and S. Cao, "Application of edge intelligent computing in satellite internet of things," in *IEEE International Conference on Smart Internet of Things (SmartIoT)*, Tianjin, China, Aug. 2019, pp. 85-91.

[6] P. D. Arapoglou, K. Liolis, M. Bertinelli, A. Panagopoulos, P. Cottis, and R. De Gaudenzi, "MIMO over satellite: A review," *IEEE Commun. Surveys and Tuts.*, vol. 13, no. 1, pp. 27-51, Mar. 2011.

[7] R. T. Schwarz, A. Knopp, D. Ogermann, C.A. Hofmann, and B. Lankl, "Optimum-capacity MIMO satellite link for fixed and mobile services," in *2008 International ITG Workshop on Smart Antennas*, Vienna, Austria, Feb. 2008, pp. 209-216.

[8] R.T. Schwarz, A. Knopp, B. Lankl, D. Ogermann, and C.A. Hofmann, "Optimum-capacity MIMO satellite broadcast system: Conceptual design for LOS channels," in *2008 4th Advanced Satellite Mobile Systems*, Bologna, Italy, Aug. 2008, pp. 60-65.

[9] C. I. Oh, S. H. Choi, D. I. Chang, and D.-G. Oh, "Analysis of the rain fading channel and the system applying MIMO," in *2006 International Symposium on Communications and Information Technologies*, Bangkok, Thailand, 2006, pp. 507-510.

[10] G. Alfano, A. De Maio, and A. M. Tulino, "A theoretical framework for LMS MIMO communication systems performance analysis," *IEEE Trans. Inf. Theory.*, vol. 56, no. 11, pp. 5614-5630, Nov. 2010.

[11] F. Lombardo, A. Vanelli-Coralli, E.A. Candreva, and G.E. Corazza, "Multi-gateway interference cancellation techniques for the return link of multi-beam broadband satellite systems," in *2012 IEEE Global Communications Conference (GLOBECOM)*, Anaheim, CA, 2012, pp. 3425-3430.

[12] P. King, *Modeling and measurement of the land mobile satellite MIMO radio propagation channel*, Ph. D. dissertation, University of Surrey, UK, Jun. 2007.

[13] P. Henarejos and A. I. Perez-Neira, "Dual polarized modulation and reception for next generation mobile satellite communications," *IEEE Trans. Commun.*, vol. 63, no. 10, pp. 3803-3812, Oct. 2015.

[14] K. P. Liolis, J. G. Vilardebo, E. Casini, and A. P. Neira, "Statistical modeling of dual-polarized MIMO land mobile satellite channels," *IEEE Trans. Commun.*, vol. 58, no. 11, pp. 3077-3083, Sept. 2010.

[15] R. P. Cerdeira, F. Perez Fontan, P. Burzigotti, A. Bolea Alamanac, and I. Sanchez Lago, "Versatile two-state land mobile satellite channel model with first application to DVB-SH analysis," *Int. J. Satell. Commun. Netw.*, vol. 28, no. 5, pp. 291-315, Dec. 2010.

[16] Y. Dhungana, N. Rajatheva, and C. Tellambura, "Dual hop MIMO OSTBC for LMS communication," *IEEE Wireless Commun. Lett.*, vol. 1, no. 2, pp. 105-108, Apr. 2012.

[17] P. Henarejos and A. I. Pĺerez-Neira, "3-D polarized modulation: System analysis and performance," *IEEE Trans. Commun.*, vol. 66, no. 11, pp. 5305-5316, Nov. 2018.

[18] Z. Luo, Z. Pei and B. Zou, "Directional polarization modulation for secure dual-polarized satellite communication," in *2019 International Conference on Communications, Information System and Computer Engineering (CISCE)*, Haikou, China, 2019, pp. 270-275.

[19] B. Zuo, K. Zhao, W. Li, and N. Zhang, "Polarized modulation scheme for mobile satellite MIMO broadcasting," in *2015 IEEE International Wireless Symposium (IWS 2015)*, Shenzhen, China, 2015, pp. 1-4.

[20] J. Zhu, P. Yang, Y. Xiao, M. Di Renzo, and S. Li, "Dual polarized spatial modulation for land mobile satellite communications," in *2018 IEEE Globecom Workshops (GC Wkshps)*, Abu Dhabi, United Arab Emirates, Dec. 2018, pp. 1-6.

[21] G. Zafari, M. Koca and H. Sari, "Dual-polarized spatial modulation over correlated fading channels," *IEEE Trans. Commun.*, vol. 65, no. 3, pp. 1336-1352, Mar. 2017.

[22] X. Chen, M. Wen, Q. Li, Y. Wu and T. A. Tsiftsis, "Dual-polarized spatial media-based modulation," *IEEE J. Sel. Topics Signal Process.*, vol. 13, no. 6, pp. 1258-1269, Oct. 2019.

[23] C. Cheng, H. Sari, S. Sezginer, and Y. T. Su, "Enhanced spatial modulation with multiple signal constellations," *IEEE Trans. Commun.*, vol. 63, no. 6, pp. 2237-2248, Jun. 2015.

[24] P. Yang, Y. Xiao, M. Xiao, J. Zhu, S. Li, and W. Xiang, "Enhanced receive spatial modulation based on power allocation," *IEEE J. Sel. Topics Signal Process.*, vol. 13, no. 6, pp. 1312-1325, Oct. 2019.

[25] P. Yang, Y. Xiao, M. Xiao, Y. L. Guan, S. Li, and W. Xiang, "Adaptive spatial modulation MIMO based on machine learning," *IEEE J. Sel. Areas Commun.*, vol. 37, no. 9, pp. 2117-2131, Sept. 2019.

[26] C. Liaskos, S. Nie, A. Tsioliaridou, A. Pitsillides, S. Ioannidis, and I. Akyildiz, "A new wireless communication paradigm through software-controlled metasurfaces," *IEEE Commun. Mag.*, vol. 56, no. 9, pp. 162-169, Sept. 2018.

[27] M. D. Renzo et al.,"Smart radio environments empowered by reconfigurable intelligent surfaces: How it works, state of research, and road ahead," *IEEE J. Sel. Areas Commun.*, 2020, in press, DoI: 10.1109/JSAC.2020.3007211.

[28] E. Basar, M. Di Renzo, J. De Rosny, M. Debbah, M. Alouini, and R. Zhang, "Wireless communications through reconfigurable intelligent surfaces," *IEEE Access*, vol. 7, pp. 116753-116773, Aug. 2019.

[29] Q. Wu, S. Zhang, B. Zheng, C. You, and R. Zhang, "Intelligent reflecting surface aided wireless communicatiuons: A tutorial," *arXiv preprint arXiv: 2007.02759*, 2020.

[30] T. Hou, Y. Liu, Z. Song, X. Sun and Y. Chen, "MIMO-NOMA networks relying on reconfigurable intelligent surface: A signal cancellation-based design," *IEEE Trans. Commun.*, vol. 68, no. 11, pp. 6932-6944, Nov. 2020.

[31] E. Lagunas, S. K. Sharma, S. Maleki, S. Chatzinotas, and B. Ottersten, "Resource allocation for cognitive satellite communications with incumbent terrestrial networks," *IEEE Trans. Cogn. Commun. Netw.*, vol. 1, no. 3, pp. 305-317, Sept. 2015.

[32] Y. Ruan, Y. Li, C. Wang, R. Zhang, and H. Zhang, "Power allocation in cognitive satellite-vehicular networks from energy-spectral efficiency tradeoff perspective," *IEEE Trans. Cogn. Commun. Netw.*, vol. 5, no. 2, pp. 318-329, Jun. 2019.

[33] M. Lee, W. Chung, and T. Lee, "Generalized precoder design formulation and iterative algorithm for spatial modulation in MIMO systems with CSIT," *IEEE Trans. Commun.*, vol. 63, no. 4, pp. 1230-1244, Apr. 2015.

[34] D. S. Shiu, G. Foschini, M. Gans, and J. Kahn, "Fading correlation and its effect on the capacity of multielement antenna systems," *IEEE Trans. Commun.*, vol. 48, no. 3, pp. 502-513, Mar. 2000.

[35] M. Di Renzo and H. Haas,"Bit error probability of SM-MIMO over generalized fading channels" *IEEE Trans. Veh. Technol.*, vol. 61, no. 3, pp. 1124-1144, Mar. 2012.

[36] L. Sanguinetti, A. Zappone and M. Debbah, "Deep learning power allocation in massive MIMO," in *Proc. Asilomar Conf. Signals, Syst., Comput.*, Pacific Grove, CA, USA, Oct. 2018, pp. 1257-1261.

Liangxin Qian received his bachelor's degree in communication engineering in 2019 from the University of Electronic Science and Technology of China, Chengdu, China, where he is working toward the masteraís degree. His research interests include multiple-input, multiple-output, machine learning, and index modulation technologies.

Ping Yang [M'13, SM'16] received the B.S. (with first class Hons.), M.S. and Doctor of Philosophy (Ph.D.) degrees from the University of Electronic Science and Technology of China (UESTC), Sicuan, China, in 2006, 2009, and 2013, respectively. From 2012 to 2013, he was a visiting student at the School of Electronics and Computer Science, University of Southampton, United Kingdom. From 2014 to 2016, he was a research fellow at the School of Electrical and Electronic Engineering, Nanyang Technological University, Singapore. Currently, he is a full professor at UESTC. His research interests include machine learning, life science and communication signal processing. He has authored over more than 100 papers in IEEE journals and conference proceedings as well as a book "Spatial Modulation for Multiple Antennas Systems". Also, he holds 12 CN and 2 US patents and co-authored another 20+ patent applications on 5G technologies and machine learning. He has been Co-Chair /TPC member of several IEEE top-tier conferences. He received Exemplary Reviewer of IEEE Communications Letters and IEEE Transactions on Communications in 2015 and 2020, respectively. He is currently an editor of IEEE Communications Letters and Transactions on Emerging Telecom. Technologies (Wiley). He was the Lead Guest Editor of IEEE JSTSP and the Guest Editor of Frontiers in Communications and Networks.

Yong Liang Guan received his Ph.D. degree from the Imperial College of Science, Technology and Medicine, University of London, in 1997, and B.Eng. degree with first class honors from the National University of Singapore in 1991. He is now an associate professor at the School of Electrical and Electronic Engineering, Nanyang Technological University. His research interests include modulation, coding and signal processing for communication, information security and storage systems. The authorąs homepage is available online at http://www3.ntu.edu.sg/home/eylguan.

Zilong Liu is a Lecturer (Assistant Professor) at the School of Computer Science and Electronics Engineering, University of Essex. He received his PhD (2014) from School of Electrical and Electronic Engineering, Nanyang Technological University (NTU, Singapore), Master Degree (2007) in the Department of Electronic Engineering from Tsinghua University (China), and Bachelor Degree (2004) in the School of Electronics and Information Engineering from Huazhong University of Science and Technology (HUST, China). From Jan. 2018 to Nov. 2019, he was a Senior Research Fellow at the Institute for Communication Systems (ICS), Home of the 5G Innovation Centre (5GIC), University of Surrey. Prior to his career in UK, he spent nine and half years in NTU, first as a Research Associate (Jul. 2008 to Oct. 2014) and then a Research Fellow (Nov. 2014 to Dec. 2017). His PhD thesis "Perfect- and Quasi- Complementary Sequences", focusing on fundamental limits, algebraic constructions, and applications of complementary sequences in wireless communications, has settled a few long-standing open problems in the field. His research lies in the interplay of coding, signal processing, and communications, with a major objective of bridging theory and practice as much as possible. Recently, he has developed an interest in applying machine learning for wireless communications. He is a Senior Member of IEEE and an Associate Editor of IEEE Wireless Communications Letters, IEEE Access, Frontiers in Communications and Networks, and Frontiers in Signal Processing. He is a General Co-Chair of the 10th International Workshop on Signal Design and its Applications in Communications (IWSDA'2022) and a TPC Co-Chair of the 2020 IEEE International Conference on Advanced Networks and Telecommunications Systems (ATTS'2020). Besides, he was/is a TPC member of a number of IEEE Conferences/Workshops (e.g., ICC, WCSP, GLOBECOM, ICCS, SETA). Details of his research can be found at: https://sites.google.com/site/zilongliu2357.

Yue Xiao received a Ph.D degree in communication and information systems from the University of Electronic Science and Technology of China in 2007. He is now an full professor at University of Electronic Science and Technology of China. He has published more than 80 international journals and been involved in several projects in Chinese Beyond 3G Communication R&D Program. His research interests are in the area of wireless and mobile communications.

Ke Jiang received his B.E. degree (with first class Hons.) in Communications Engineering from the School of Computer Science of China West Normal University (CWNU), Sichuan, China in 2016, and MA.Eng degree in Digital and Communication Engineering from the National Key Laboratory of Science and Technology on Communications of University of Electronic Science and Technology of China (UESTC), Sicuan, China in 2020. His research interests are in the areas of signal processing, signal detection, and performance analysis of MIMO-OFDM wireless communications, index modulation technologies.

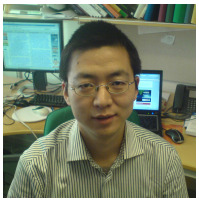

Ming Xiao (S'2002-M'2007-SM'2012) received Bachelor and Master degrees in Engineering from the University of Electronic Science and Technology of China, ChengDu in 1997 and 2002, respectively. He received Ph.D degree from Chalmers University of technology, Sweden in November 2007. From 1997 to 1999, he worked as a network and software engineer in ChinaTelecom. From 2000 to 2002, he also held a position in the SiChuan communications administration. From November 2007 to now, he has been in the department of information science and engineering, school of electrical engineering and computer science, Royal Institute of Technology, Sweden, where he is currently an Associate Professor. Since 2012, he was an Editor for IEEE Transactions on Communications (2012-2017), IEEE Communications Letters (Senior Editor Since Jan. 2015) and IEEE Wireless Communications Letters (2012-2016), and has been an Editor for IEEE Transactions on Wireless Communications since 2018. He was the lead Guest Editor for IEEE JSAC Special issue on "Millimeter Wave Communications for future mobile networks" in 2017.